

Restricted Boltzmann machine network versus Jastrow correlated wave function for the two-dimensional Hubbard model

Karthik V.* and Amal Medhi†

Indian Institute of Science Education and Research Thiruvananthapuram, Kerala 695551, India

We consider a restricted Boltzmann Machine (RBM) correlated BCS wave function as the ground state of the two-dimensional Hubbard model and study its electronic and magnetic properties as a function of hole doping. We compare the results with those obtained by using conventional Jastrow projectors. The results show that the RBM wave function outperforms the Jastrow projected ones in the underdoped region in terms of the variational energy. Computation of superconducting (SC) correlations in the model shows that the RBM wave function gives slightly weaker SC correlations as compared to the Jastrow projected wave functions. A significant advantage of the RBM wave function is that it spontaneously gives rise to strong antiferromagnetic (AF) correlations in the underdoped region even though the wave function does not incorporate any explicit AF order. In comparison, AF correlations in the Jastrow projected wave functions are found to be very weak. These and other results obtained show that the RBM wave function provides an improved description of the phase diagram of the model. The work also demonstrates the power of neural-network quantum state (NQS) wave functions in the study of strongly correlated electron systems.

I. INTRODUCTION

The neural-network quantum state (NQS) wave functions have recently been applied successfully to study several quantum many-body systems[1–6]. The NQS wave functions are variational wave functions constructed based on an artificial neural-networks (ANNs). The power of such wave functions derives from the expressive capability of the ANNs which can represent highly nonlinear functions[7]. In contrast to the traditional Jastrow-type variational wave functions[8–10] which are biased by the choice of a mean-field ansatz, NQS wave functions can be highly unbiased and can provide an accurate representation of quantum many-body states as has been demonstrated in several works[2, 5, 11–15]. However, most of these applications have been limited to bosonic systems. For fermionic systems, there is a key disadvantage that though neural-networks can represent complicated functions, it generally fails to take into account the complicated sign structure of a fermionic many-body wave function[16, 17]. Indeed, it fails to correctly represent the sign structures of the wave function of even non-interacting fermions[17]. An alternative approach in which the above problem is avoided is to use an ANN as a correlator to an antisymmetric one-body wave function which takes care of the fermionic symmetry correctly. Although such a wave function is less unbiased by construction, it still outperforms traditional Jastrow projected wave functions in terms of accuracy. For example, Nomura *et al.*[18] have used the restricted Boltzmann machine (RBM) network as a correlator to a generalized pair-product wave function. The resulting RBM+PP wave function was shown to give significantly lower energy compared to Jastrow type wave function for the two-dimensional Hubbard model at half-filling. In a recent work[19], the present authors showed that a convolutional restricted Boltzmann machine (CRBM) correlated wave function provides a significantly improved description of the

ground state of the half-filled Hubbard model on a square lattice.

In this work, we consider an RBM correlated BCS wave function as a ground state of the two-dimensional Hubbard model and study it as a function of hole doping. We examine several electronic properties like ground state energy, superconducting and magnetic correlations etc. and compare the results with those obtained by using several standard Jastrow projectors. Specifically, the wave function we consider is of the form $\mathcal{P}|BCS\rangle_N$, where $|BCS\rangle_N$ is the BCS state with fixed electron number and \mathcal{P} is the projector or the correlator which introduces electronic correlation into the wave function. We take it to be \mathcal{P}_{RBM} , a correlator constructed using an RBM network as well as three other Gutzwiller-Jastrow projectors. We study the resulting wave function using the variational Monte Carlo method[20–22]. We show that compared to the Jastrow projectors, the RBM correlated wave function gives lower energy in the underdoped phase of the model. We obtain a ground state phase diagram of the model and show that the wave function give a better description of the superconducting and magnetic properties of the model. The rest of the paper is organized as follows. We describe the model and the variational wave functions considered in section II. The results are described in section III. Finally, we give the summary and concluding remarks in section IV.

II. MODEL AND METHOD

We consider the fermionic Hubbard model on a two-dimensional (2D) square lattice given by,

$$\mathcal{H} = -t \sum_{\langle i,j \rangle \sigma} (c_{i\sigma}^\dagger c_{j\sigma} + hc) + U \sum_i n_{i\uparrow} n_{i\downarrow} \quad (1)$$

The operator $c_{i\sigma}^\dagger$ creates an electron at site ‘ i ’ with spin σ , and $c_{i\sigma}$ is the corresponding annihilation operator. $n_{i\sigma} = c_{i\sigma}^\dagger c_{i\sigma}$ is the number operator. In the first term, the summation is over the nearest-neighbor sites. The parameter t is the hopping amplitude and U is the onsite Hubbard repulsive potential. Here

* karthik.v16@iisertvm.ac.in

† amedhi@iisertvm.ac.in

we take $U/t = 8$, a value that lies in the intermediate coupling strength regime of the model.

The RBM correlated wave function we consider is given by,

$$|\Psi_{RBM}\rangle = \mathcal{P}_{RBM} |BCS\rangle_N \quad (2)$$

where $|BCS\rangle_N$ is the BCS ground state in the subspace of the fixed number of particles ($2N$), of the following mean-field pairing Hamiltonian,

$$\mathcal{H}_{MF} = \sum_{\mathbf{k}\sigma} \varepsilon_{\mathbf{k}} c_{\mathbf{k}\sigma}^\dagger c_{\mathbf{k}\sigma} + \sum_{\mathbf{k}} \left(\Delta_{\mathbf{k}} c_{\mathbf{k}\uparrow}^\dagger c_{-\mathbf{k}\downarrow}^\dagger + hc \right) \quad (3)$$

where $\varepsilon_{\mathbf{k}} = -2t(\cos k_x + \cos k_y) - \mu$. We take the superconducting (SC) pair amplitude to be $\Delta_{\mathbf{k}} = \Delta_{SC}(\cos k_x - \cos k_y)$ (d -wave pairing). The quantities Δ_{SC} and μ are the variational parameters in the mean-field part of the wave function. The BCS wave function in real-space representation can be written as,

$$|BCS\rangle_N = \sum_{\{i_1, \dots, i_N, j_1, \dots, j_N\}} \begin{vmatrix} \phi(\mathbf{r}_{i_1} - \mathbf{r}_{j_1}) & \dots & \phi(\mathbf{r}_{i_1} - \mathbf{r}_{j_N}) \\ \vdots & \dots & \vdots \\ \phi(\mathbf{r}_{i_N} - \mathbf{r}_{j_1}) & \dots & \phi(\mathbf{r}_{i_N} - \mathbf{r}_{j_N}) \end{vmatrix} \times c_{i_1\uparrow}^\dagger \dots c_{i_N\uparrow}^\dagger c_{j_1\downarrow}^\dagger \dots c_{j_N\downarrow}^\dagger |0\rangle \quad (4)$$

The set $\{i_1, \dots, i_N, j_1, \dots, j_N\}$ represent the set of sites occupied by the electrons. The pair amplitudes $\phi(\mathbf{r}_i - \mathbf{r}_j)$ are functions of the variational parameters Δ_{SC} and μ [23]. Denoting the determinantal coefficients by Ψ_{BCS} , we can write,

$$\begin{aligned} |BCS\rangle_N &= \sum_{n_1, n_2, \dots, n_{2L}} \Psi_{BCS}(n_1, n_2, \dots, n_{2L}) \\ &\quad \times (c_{1\uparrow}^\dagger)^{n_1} \dots (c_{L\uparrow}^\dagger)^{n_L} (c_{1\downarrow}^\dagger)^{n_{L+1}} \dots (c_{L\downarrow}^\dagger)^{n_{2L}} |0\rangle \\ &= \sum_R \Psi_{BCS}(R) |R\rangle \end{aligned} \quad (5)$$

The occupation number n_i -s can values 0 or 1. L is the number of lattice sites. The set $R \equiv \{n_1, n_2, \dots, n_{2L}\}$ specifies the electronic configurations.

Now we consider a restricted Boltzmann machine (RBM) network as shown in Fig. 1. The network consists of a visible

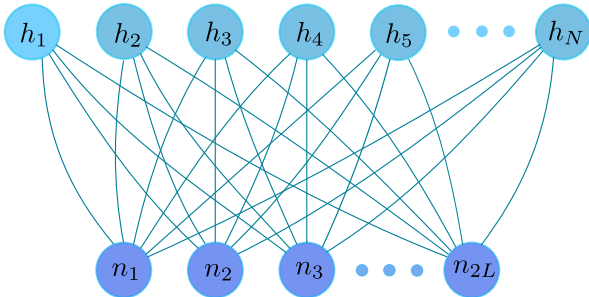


FIG. 1. Schematic diagram of a restricted Boltzmann machine (RBM) network. The input to the network are the electron occupation numbers $\{n_1, n_2, \dots, n_{2L}\}$. The hidden layer defines variables h_i which can take values ± 1 .

layer with $2L$ neurons and a hidden layer with $P = 2L\alpha$ neurons. The parameter α is called the hidden variable density.

Let a_i, b_j be the bias parameters corresponding to the neurons in the visible and hidden layers, respectively. Also, let w_{ij} be the weight parameter corresponding to the connection between i -th visible neuron and the j -th hidden. For a given input configuration $R = \{n_1, n_2, \dots, n_{2L}\}$, the RBM network defines a function[24],

$$\Psi_{RBM}(R) = \frac{1}{Z} e^{\sum_i a_i n_i} \prod_j 2 \cosh\left(\sum_i w_{ij} n_i + b_j\right) \quad (6)$$

Therefore, we define the RBM variational wave function as,

$$|\Psi_{RBM}\rangle = \mathcal{P}_{RBM} |BCS\rangle_N = \sum_R \Psi_{RBM}(R) \Psi_{BCS}(R) |R\rangle \quad (7)$$

where the network parameters a_i, b_j, w_{ij} are treated as the variational parameters. The number of parameters can be greatly reduced by incorporating the symmetries of the Hamiltonian into the wave function. Here we use the lattice translational symmetry and impose the condition that for two electronic configurations R and R' connected by a lattice translation operation, the corresponding wave function amplitudes are equal, i.e. $\Psi_{RBM}(R) = \Psi_{RBM}(R')$. This reduces the numbers of w_{ij} and b_j parameters to $4L$ and 2 , respectively. Also since we are working with fixed electron number representation, the sum $\sum_i a_i n_i$ is a constant, and the factor $e^{\sum_i a_i n_i}$ can be dropped from the Eq. (6). Thus total number of variational parameters becomes $(4L + 2)$.

For comparison, we also obtain results for the following Jastrow projected wave functions. The first is the Gutzwiller (GW) projected wave function $|\Psi_{GW}\rangle = \mathcal{P}_G |BCS\rangle_N$, where

$$\mathcal{P}_G = \prod_i [1 - (1 - g)n_{i\uparrow}n_{i\downarrow}], \quad 0 < g \leq 1 \quad (8)$$

The second wave function we consider is given by $|\Psi_{GW+DH}\rangle = \mathcal{P}_G \mathcal{P}_{DH} |BCS\rangle_N$. It incorporates doublon (DH) binding with \mathcal{P}_{DH} given by[25],

$$\begin{aligned} \mathcal{P}_{DH} &= \prod_i (1 - \eta Q_i) \\ Q_i &= \prod_{\delta} [d_i(1 - h_{i+\delta}) + h_i(1 + d_{i+\delta})] \end{aligned} \quad (9)$$

where $d_i = n_{i\uparrow}n_{i\downarrow}$ is doublon and $h_i = (1 - n_{i\uparrow})(1 - n_{i\downarrow})$ is holon operator. δ denotes the nearest-neighbor sites, and η is a variational parameter. We also consider the long range density-density projected Jastrow wave function given by $|\Psi_{Jastrow}\rangle = \mathcal{P}_J |BCS\rangle_N$, where

$$\mathcal{P}_J = \exp\left(\sum_{ij} \frac{1}{2} v_{ij} (n_i - 1)(n_j - 1) + w_{ij} h_i d_j\right) \quad (11)$$

Here the quantities v_{ij} and w_{ij} are variational parameters.

We use the variational Monte Carlo (VMC) method[20, 21, 26] to compute the variational energy,

$$E_{var}(\boldsymbol{\alpha}) = \frac{\langle \Psi_{var} | \mathcal{H} | \Psi_{var} \rangle}{\langle \Psi_{var} | \Psi_{var} \rangle} \quad (12)$$

The wave functions are optimized by minimizing $E_{var}(\boldsymbol{\alpha})$ with respect to the variational parameters $\boldsymbol{\alpha}$. We use the stochastic reconfiguration (SR) technique[20, 21] for the purpose.

III. RESULTS

We consider a lattice of size $L = 8 \times 8$. The Hubbard interaction parameter is fixed at $U/t = 8$. The RBM wave function depends upon the network structural parameter, that is the hidden variable density α . We need to fix the value of α before going ahead with the calculations. We determine α by repeatedly optimizing the variational energy for a given model parameters by taking different values of α . The results obtained at two different hole dopings are shown in Fig. 2(a). As the

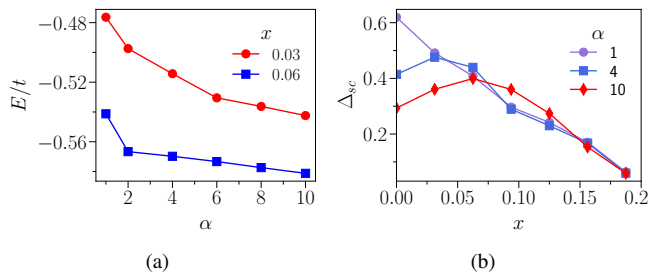


FIG. 2. (a) Optimized variational energy of the RBM-SC wave function as a function of network hidden variable density α . (b) Variation of optimized SC gap parameter Δ_{SC} with hole doping x at three different values of α . The variation becomes dome shaped at large α .

figure shows, the variational energy decreases with increasing α implying more accurate wave function for larger α . However, increasing α also raises the computational complexity as the number of variational parameters increases rapidly with α . Thus, one needs to make a trade-off between accuracy and computational efficiency. Here, we fix the parameter at $\alpha = 10$ for the rest of the calculations, a value that gives good balance between accuracy and efficiency. Fig. 2(b) shows the doping dependence of the optimized SC gap parameter Δ_{SC} at different α . It is interesting to note that at large α , where the WF becomes more accurate, the variation of optimal gap parameter Δ_{SC} as a function hole doping x changes qualitatively. The variation becomes dome shaped at large α .

Having fixed the network parameters, we optimize the wave function as a function of hole doping x . First, we examine how the energy of the RBM wave function, $|\Psi_{RBM}\rangle$ compares with those for the three Jastrow-type wave functions, e.g. $|\Psi_{GW}\rangle$, $|\Psi_{GW+DH}\rangle$, and $|\Psi_{Jastrow}\rangle$ defined in the previous section. The comparison of energy is shown in Fig. 3(a). Fig. 3(b) shows the energy of the other three wave functions relative to GW energy for clarity. As the figure shows, the GW wave function has the highest energy. As observed in previous studies, the simple GW projector does not take into account correlations effects adequately and hence is rather a poor approximation to the ground state especially for large U [25, 27–29]. Taking the doublon-holon (DH) binding into account improves the wave function substantially as energy as the curve for GW+DH shows. The energies of the GW+DH and the long range density-density Jastrow projected WFs are significantly lower than the GW energy. The RBM wave function gives the lowest energy and hence the most accurate among the four. Indeed, the RBM projector captures the correlation

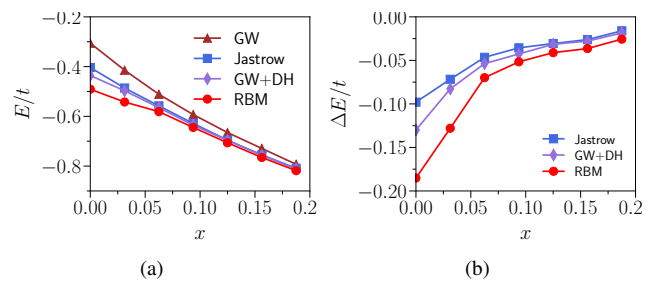


FIG. 3. (a) Optimized variational energy (per site) for the four wave functions shown as a function of hole doping x . (b) The energy $\Delta E/t = E_X/t - E_{GW}/t$ relative to the GW energy as a function of x . Here X stands for Jastrow or GW+DH or RBM. $U/t = 8$.

effect better, especially in the underdoped region where it also displays strong antiferromagnetic (AF) correlations as shown below.

To examine the magnetic order, we calculate the spin-spin correlation function and spin structure factor $S(\mathbf{q})$ given by,

$$S(\mathbf{q}) = \frac{1}{L^2} \sum_{i,j} e^{i\mathbf{q}\cdot(\mathbf{r}_i - \mathbf{r}_j)} \langle S_i^z S_j^z \rangle \quad (13)$$

where $S_i^z = (n_{i\uparrow} - n_{i\downarrow})$ is the z -component of the spin operator at site i . Fig. 4(a) shows the results for $S(\mathbf{q})$ as a function of \mathbf{q} along the Brillouin zone symmetry path for the RBM wave function at various hole dopings. As the figure shows,

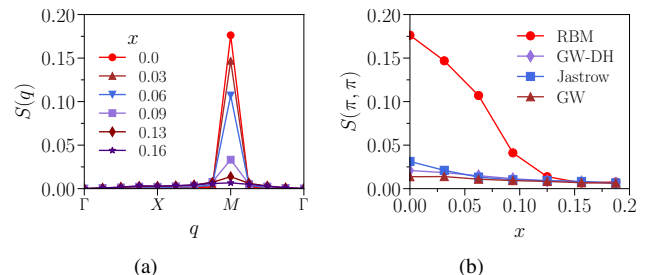


FIG. 4. (a) Spin structure factor $S(\mathbf{q})$ versus \mathbf{q} along the symmetry path in the Brillouin zone of the lattice for the RBM wave function, at various values of hole doping x . (b) Comparison of the staggered structure factor $S(\pi, \pi)$ at various x for the four wave functions.

$S(\mathbf{q})$ peaks sharply at $\mathbf{q} = (\pi, \pi)$ suggesting strong AF order in the wave function, especially the underdoped region. The peak is maximum at half-filling and drops rapidly with hole doping becoming very small for $x \gtrsim 0.1$. The strong AF order in the wave function is interesting given the fact that the mean-field part of the wave function, e.g., $|BCS\rangle_N$ does not have any explicit symmetry broken AF order. This is not the case with the Jastrow-type projectors which give very weak AF correlations if the mean-field part itself does not have an explicit AF order as is the case here. This is clearly evident from Fig. 4(b) which shows comparison of $S(\pi, \pi)$ values for the four wave functions. The AF degrees of freedom in the RBM wave function can be easily understood if we look at

the form of the RBM amplitude given in Eq. (6). The amplitudes depends upon the matrix-vector product $W^T \bar{n}$ which can be written as, $[W_\uparrow \ W_\downarrow] \begin{bmatrix} \bar{n}_\uparrow \\ \bar{n}_\downarrow \end{bmatrix}$ where $W_{\uparrow,\downarrow}$ matrices are of size $2L \times L$, and $\bar{n}_{\uparrow,\downarrow}$ are $L \times 1$ vectors representing occupation numbers of the spin- \uparrow and spin- \downarrow states. The elements (variational parameters) of the two sub-matrices W_\uparrow and W_\downarrow are independent of each other even after the imposition of lattice translational symmetry. Therefore, the elements in the first and second half of the product vector $W^T \bar{n}$ are also distinct. Thus the weights Ψ_{RBM} from the RBM network are spin-resolved by construction which distinguishes between different spin-configurations. These variational degrees of freedom make it possible to obtain AF spin configuration in the wave function upon optimization of the parameters.

We calculate the charge structure factor $N(\mathbf{q})$ given by,

$$N(\mathbf{q}) = \frac{1}{L^2} \sum_{i,j} e^{i\mathbf{q} \cdot (\mathbf{r}_i - \mathbf{r}_j)} \langle n_i n_j \rangle - n^2 \quad (14)$$

The quantity calculated at various hole doping for the RBM-SC wave function is shown in Fig. 5. As the figure shows,

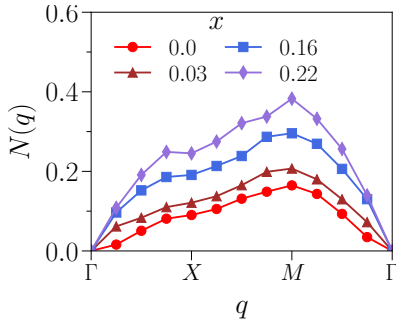


FIG. 5. Charge structure factor $N(\mathbf{q})$ as a function of $|\mathbf{q}|$ for the RBM wave function at various hole dopings.

$N(\mathbf{q})$ is the smallest at half-filling. It increases as we increase the hole doping x . At half-filling, $N(\mathbf{q}) \rightarrow |\mathbf{q}|^2$ for small $|\mathbf{q}|$ indicating the presence of charge gap. As soon as we dope the system, this behavior of $N(\mathbf{q})$ changes and it goes as $N(\mathbf{q}) \rightarrow |\mathbf{q}|$, when $|\mathbf{q}| \rightarrow 0$. Thus the system becomes metallic for $x > 0$.

Next, we calculate the superconducting pair-pair correlation function given by,

$$F_{\alpha,\beta}(\mathbf{r} - \mathbf{r}') = \langle B_{r\alpha}^\dagger B_{r'\beta} \rangle \quad (15)$$

where $B_{r\alpha}^\dagger = \frac{1}{\sqrt{2}} (c_{r\uparrow}^\dagger c_{r+\hat{\alpha}\downarrow}^\dagger - c_{r\downarrow}^\dagger c_{r+\hat{\alpha}\uparrow}^\dagger)$ creates an electron singlet on the bond $(\mathbf{r}, \mathbf{r} + \hat{\alpha})$ and α, β can take values \hat{x} or \hat{y} . We estimate the SC order parameter Φ_{sc} as $F_{\alpha,\beta}(\mathbf{r} - \mathbf{r}') \rightarrow \pm \Phi_{sc}^2$ for large $|\mathbf{r} - \mathbf{r}'|$, with the sign being $+$ ($-$) for $\alpha \parallel \beta$ ($\alpha \perp \beta$). Fig. 6 shows the order parameter as a function hole doping for various wave functions, which shows the familiar dome shaped variation of Φ_{sc} with x . The GW wave function clearly overestimates the strength of SC correlations in the

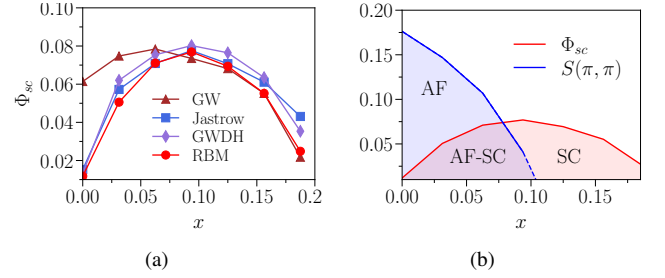


FIG. 6. (a) Superconducting order parameter Φ_{sc} as a function hole doping x for various wave functions. (b) Schematic phase diagram of the model showing regions of SC and AF ordering as obtained from the RBM wave function.

underdoped region, even giving a non-vanishing Φ_{sc} at half-filling. This is obviously due to the failure of the GW projector to take into account electron correlation effects adequately. For the other three wave functions, Φ_{sc} is roughly of similar magnitudes, except for in the underdoped region where Φ_{sc} is marginally on the lower side for the RBM wave function. As described above, the RBM wave function also displays strong AF correlations in the underdoped region whereas it is very weak for the other wave functions. Given the fact that Φ_{sc} is roughly the same for these wave functions, it follows that the SC correlations are unaffected by the presence of AF order. Having obtained the value of SC and AF order parameters in the RBM wave function, we obtain a superconducting phase diagram as a function of hole doping which is shown in Fig. 6(b). As depicted in the figure, the ground state is AF insulating at half-filling. Away from half-filling, it becomes superconducting with Φ_{sc} becoming maximum at around $x \sim 0.1$. Antiferromagnetism coexists with superconductivity in the underdoped region. Φ_{sc} decreases gradually in the overdoped region and vanishes at around $x \sim 0.2$. The phase diagram qualitatively agrees with the results found by other studies that include the AF order in the mean-field state[23, 25, 30].

Finally, we look at the momentum distribution function $n(\mathbf{k}) = \langle c_{\mathbf{k}\sigma}^\dagger c_{\mathbf{k}\sigma} \rangle$ in the wave functions. The values of $n(\mathbf{k})$ for the four wave functions are shown in Fig. 7 for three different hole dopings. Since our lattice size and hence the number of data points are rather small, it is difficult to make an accurate comparison. Nevertheless, the results suggest that at $x = 0$, the $n(\mathbf{k})$ curve for the RBM wave function is a smooth one without having any discontinuity as it should be for a Mott insulating state. The curves for the Jastrow wave functions are somewhat qualitatively different. Here the shift in $n(\mathbf{k})$ weights from the Brillouin zone center, Γ to zone center M is somewhat more stronger. At $x = 0.06$ in the underdoped region, $n(\mathbf{k})$ for the Jastrow wave functions shows a clear jump at the Fermi wave vector in the nodal $\Gamma - M$ direction. In contrast, the curve for the RBM wave function remains smooth signifying non-Fermi liquid nature of the state in the underdoped region. At the overdoped value $x = 0.19$, the curves for all the wave functions merge with each other showing once again that the wave functions become equivalent in this re-

gion.

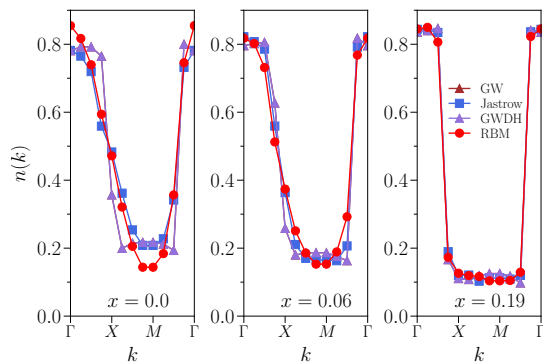


FIG. 7. Momentum distribution $n(\mathbf{k})$ for the four wave functions shown in figure as a function of \mathbf{k} along the symmetry path in the Brillouin zone, at three different values of hole doping x .

IV. SUMMARY

In summary, we have considered an NQS wave function obtained by using the RBM network as a correlator to the BCS wave function and used it to study the ground state of the Hubbard model as a function of hole doping. The wave functions considered are of the form $\mathcal{P}|BCS\rangle_N$, where \mathcal{P} is a projection operator and $|BCS\rangle_N$ is the BCS wave function of an underlying mean-field Hamiltonian. Different choices of the projector \mathcal{P} we considered are \mathcal{P}_{RBM} , \mathcal{P}_{GW} , \mathcal{P}_{GW+DH} , and $\mathcal{P}_{Jastrow}$. The first one is constructed using an RBM network whereas the last three are conventional Jastrow projectors. We examined several properties of the model using these

wave functions and made a detailed comparison among them. We found the RBM correlated wave function to be most accurate in terms of ground state energy as compared to the Jastrow projected ones, especially in the underdoped region of the model. At half-filling, all the wave functions except for the GW projected one describes a Mott insulating state. Superconductivity appears away from half-filling. The most interesting feature is that while all the Jastrow projected wave function describes a weak antiferromagnetic (AF) order, the AF corrections in the RBM wave function is found to be very strong, even though the mean-field part of the wave function does not contain any explicit magnetic order. This occurs as the RBM network naturally generates spin-resolved weights by construction. Overall, the RBM projector offers an improved description of the ground state. On the flip side, the RBM network though is a computationally efficient neural-network framework, it still involves significantly higher computational difficulty, especially in optimization, as the number of variational parameters grows rapidly with the system size. Therefore, it is desirable to explore other network architectures for better computational efficiency and significantly higher accuracy. We considered the convolutional restricted Boltzmann machine (CRBM) network which was found to be much more accurate and computationally efficient for the model at half-filling[19], but encountered issues with numerical stability during optimization away from half-filling.

ACKNOWLEDGEMENT

The authors thank Anusandhan National Research Foundation (ANRF), Govt of India for financial support under the Core grant (No: CRG/2021/005792). Also acknowledge CHPC, IISER Thiruvananthapuram for computational facilities.

-
- [1] J. Carrasquilla and R. G. Melko, Machine learning phases of matter, *Nature Physics* **13**, 431–434 (2017).
 - [2] G. Carleo and M. Troyer, Solving the quantum many-body problem with artificial neural networks, *Science* **355**, 602–606 (2017).
 - [3] E. P. L. van Nieuwenburg, Y.-H. Liu, and S. D. Huber, Learning phase transitions by confusion, *Nature Physics* **13**, 435–439 (2017).
 - [4] P. Broecker, J. Carrasquilla, R. G. Melko, and S. Trebst, Machine learning quantum phases of matter beyond the fermion sign problem, *Scientific Reports* **7**, 8823 (2017).
 - [5] K. Ch’ng, J. Carrasquilla, R. G. Melko, and E. Khatami, Machine learning phases of strongly correlated fermions, *Phys. Rev. X* **7**, 031038 (2017).
 - [6] D.-L. Deng, X. Li, and S. Das Sarma, Quantum entanglement in neural network states, *Phys. Rev. X* **7**, 021021 (2017).
 - [7] K. Hornik, M. Stinchcombe, and H. White, Multilayer feedforward networks are universal approximators, *Neural Networks* **2**, 359 (1989).
 - [8] K. Yamaji, T. Yanagisawa, T. Nakanishi, and S. Koike, Variational monte carlo study on the superconductivity in the two-dimensional hubbard model, *Physica C: Superconductivity* **304**, 225 (1998).
 - [9] B. Edegger, V. N. Muthukumar, and C. Gros, Gutzwiller–rvb theory of high-temperature superconductivity: Results from renormalized mean-field theory and variational monte carlo calculations, *Advances in Physics* **56**, 1033 (2007).
 - [10] H.-H. Zhao, K. Ido, S. Morita, and M. Imada, Variational monte carlo method for fermionic models combined with tensor networks and applications to the hole-doped two-dimensional hubbard model, *Phys. Rev. B* **96**, 085103 (2017).
 - [11] K. Choo, G. Carleo, N. Regnault, and T. Neupert, Symmetries and many-body excitations with neural-network quantum states, *Phys. Rev. Lett.* **121**, 167204 (2018).
 - [12] G. Carleo, I. Cirac, K. Cranmer, L. Daudet, M. Schuld, N. Tishby, L. Vogt-Maranto, and L. Zdeborová, Machine learning and the physical sciences, *Rev. Mod. Phys.* **91**, 045002 (2019).

- [13] J. Carrasquilla, Machine learning for quantum matter, *Advances in Physics: X* **5**, 1797528 (2020), <https://doi.org/10.1080/23746149.2020.1797528>.
- [14] R. G. Melko, G. Carleo, J. Carrasquilla, and J. I. Cirac, Restricted boltzmann machines in quantum physics, *Nature Physics* **15**, 887 (2019).
- [15] J. Carrasquilla and G. Torlai, How to use neural networks to investigate quantum many-body physics, *PRX Quantum* **2**, 040201 (2021).
- [16] K. Inui, Y. Kato, and Y. Motome, Determinant-free fermionic wave function using feed-forward neural networks, *Phys. Rev. Res.* **3**, 043126 (2021).
- [17] Z. Cai and J. Liu, Approximating quantum many-body wave functions using artificial neural networks, *Phys. Rev. B* **97**, 035116 (2018).
- [18] Y. Nomura, A. S. Darmawan, Y. Yamaji, and M. Imada, Restricted boltzmann machine learning for solving strongly correlated quantum systems, *Phys. Rev. B* **96**, 205152 (2017).
- [19] K. V. and A. Medhi, Convolutional restricted boltzmann machine correlated variational wave function for the hubbard model on a square lattice, *Phys. Rev. B* **110**, 125125 (2024).
- [20] D. Tahara and M. Imada, Variational monte carlo method combined with quantum-number projection and multi-variable optimization, *Journal of the Physical Society of Japan* **77**, 114701 (2008), <https://doi.org/10.1143/JPSJ.77.114701>.
- [21] S. Sorella, in *Strongly Correlated Systems*, Springer Series in Solid-State Sciences, Vol. 176, edited by A. Avella and F. Mancini (Springer, Berlin, Heidelberg, 2013) Chap. Variational Monte Carlo and Markov Chains for Computational Physics.
- [22] H. SHIBA and H. YOKOYAMA, Variational monte carlo studies of highly correlated electron systems, in *Proceedings of the Yamada Conference XVIII on Superconductivity in Highly Correlated Fermion Systems*, edited by M. Tachiki, Y. Muto, and S. Maekawa (Elsevier, 1987) pp. 264–267.
- [23] A. Paramekanti, M. Randeria, and N. Trivedi, High- T_c superconductors: A variational theory of the superconducting state, *Phys. Rev. B* **70**, 054504 (2004).
- [24] G. Carleo, Y. Nomura, and M. Imada, Constructing exact representations of quantum many-body systems with deep neural networks, *Nature Communications* **9**, 5322 (2018).
- [25] H. Yokoyama, M. Ogata, and Y. Tanaka, Mott transitions and d-wave superconductivity in half-filled-band hubbard model on square lattice with geometric frustration, *Journal of the Physical Society of Japan* **75**, 114706 (2006).
- [26] D. Ceperley, G. V. Chester, and M. H. Kalos, Monte carlo simulation of a many-fermion study, *Phys. Rev. B* **16**, 3081 (1977).
- [27] T. A. Kaplan, P. Horsch, and P. Fulde, Close relation between localized-electron magnetism and the paramagnetic wave function of completely itinerant electrons, *Phys. Rev. Lett.* **49**, 889 (1982).
- [28] M. Capello, F. Becca, M. Fabrizio, S. Sorella, and E. Tosatti, Variational description of mott insulators, *Phys. Rev. Lett.* **94**, 026406 (2005).
- [29] M. Capello, F. Becca, S. Yunoki, and S. Sorella, Unconventional metal-insulator transition in two dimensions, *Phys. Rev. B* **73**, 245116 (2006).
- [30] L. F. Tocchio, F. Becca, and S. Sorella, Hidden mott transition and large- u superconductivity in the two-dimensional hubbard model, *Phys. Rev. B* **94**, 195126 (2016).